

## Hybrid silicon-polymer platform for self-locking and self-deploying origami

Hongen Tu,<sup>1</sup> Hanqing Jiang,<sup>2</sup> Hongyu Yu,<sup>3</sup> and Yong Xu<sup>1,a)</sup>

<sup>1</sup>Department of Electrical and Computer Engineering, Wayne State University, 5050 Anthony Wayne Dr., Detroit, Michigan 48202, USA

<sup>2</sup>Mechanical Engineering, School for Engineering of Matter, Transport and Energy, Arizona State University, Tempe, Arizona 85287, USA

<sup>3</sup>School of Electrical, Computer and Energy Engineering, Arizona State University, Tempe, Arizona 85287, USA

(Received 14 September 2013; accepted 22 November 2013; published online 9 December 2013)

This Letter reports the demonstration of self-locking and self-deploying functions of an origami platform based on silicon island arrays. The silicon islands serve as the rigid part of the origami and are able to integrate complementary metal–oxide–semiconductor circuits, microelectromechanical systems, and other functional components. The creases of the origami, which are the flexible connectors among silicon islands, are realized by parylene balloons filled with paraffin wax. Metal heaters are integrated on the balloons to control the solid/liquid phases of the wax on-chip. Prototypes of such an origami platform have been fabricated. By turning on and off the heaters at different states of the origami, self-locking and self-deploying features have been demonstrated.

© 2013 AIP Publishing LLC. [<http://dx.doi.org/10.1063/1.4842235>]

Origami, traditionally the art of paper folding, has been applied to some engineering applications based on its principle of creating three-dimensional (3D) structures from two-dimensional (2D) sheets through a high degree of folding along the creases. The applications of origami ranges from space exploration (e.g., a foldable telescope lens by Gardner *et al.*<sup>1</sup>) to automotive safety (e.g., airbags) and biomedical devices (e.g., heart stent<sup>2</sup>). Many origami devices are fabricated by precision machining or laser micromachining.<sup>3</sup> More traditional microfabrication methods, such as photolithography, have been used as well.<sup>2,4–6</sup> The employment of microfabrication will potentially allow the monolithic integration of electronics and microelectromechanical systems (MEMS) sensors with origami. For this purpose, we proposed an origami platform based on microfabricated silicon island arrays. The creases among these rigid islands are realized by wax filled flexible parylene balloons. Heaters are integrated to control the phases of the filled wax, namely, solid state in low temperature and liquid state in high temperature, leading to self-locking and self-deploying features. It is worth noting that shape memory alloys have been used to realize self-foldable and self-deployable origami as well. For example, self-deployable origami stent grafts have been developed using nickel-titanium shape memory alloy.<sup>2</sup> Shape memory alloys have also been machined in the form of flat plates to achieve effective torsional actuation for origami structure.<sup>7</sup> For actuators based on shape memory alloys, a step to define their shape in hot state (austenite) is required and may pose inconvenience and incompatibility with microfabrication. Shape memory polymers and other functional polymers have also been extensively investigated for self-folding functions.<sup>8–10</sup> Due to their simplicity, heat-shrink polymers are a popular choice for self-foldable origami.<sup>6,11,12</sup> Shape memory materials or heat-shrink materials

can offer large actuation force and large deformation. However, the self-locking feature of our technology could be more convenient and provide more operation freedom. More importantly, our technology has better compatibility with silicon-based mainstream MEMS and complementary metal–oxide–semiconductor (CMOS) processes. CMOS electronics and MEMS devices, which need high-temperature processes, can be first fabricated on the silicon wafers.<sup>13–15</sup> Then low-temperature post-processes are carried out to form silicon island arrays and the parylene balloon creases. Our technology enables the monolithic integration of high-performance MEMS devices and CMOS electronics using existing processes and thus can save tremendous research efforts by avoiding re-invention. Electronics and sensors can also be integrated by packaging off-the-shelf components on the origami. However, this approach typically results in a larger volume and has a limitation in terms of the number and density of the packaged devices. The parylene-silicon platform reported in this Letter will be of great interest for many origami applications.

The proposed origami device and operation principle of self-locking and self-deployment are schematically illustrated in Fig. 1. The discrete silicon islands are connected by a parylene balloon at the creases integrated with a metal heater and filled with paraffin wax. The paraffin wax can be melted by applying electric current to the heater and return to the solid state by turning off the heater. To fold the

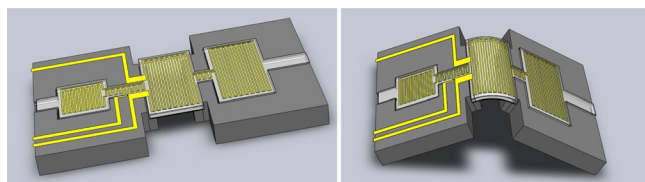


FIG. 1. Schematic of the silicon island origami with a parylene balloon crease for self-locking and self-deploying functions.

<sup>a)</sup>Author to whom correspondence should be addressed. Electronic mail: [yxu@eng.wayne.edu](mailto:yxu@eng.wayne.edu)

origami, the wax is melted first, making the balloon flexible. Then, the device is folded by external forces. While the device is kept in the folded state, the heater is turned off. The wax solidifies and the origami is locked in the folded state. For the deployment, the heater is turned on to melt the wax to the liquid state. Thus, the folded origami can return to its original flat state when the heater is on due to the elastic restoring force of the parylene balloon.

The simplified fabrication is illustrated in Fig. 2. A  $500\ \mu\text{m}$  thick silicon wafer was used for the fabrication. First, the wafer was thoroughly cleaned and deposited with  $3\ \mu\text{m}$  thick parylene C layer as shown in Fig. 2(a). Then, as shown in Fig. 2(b), a layer of  $25/200\ \text{nm}$  Ti/Au layer was deposited and patterned to form the micro heaters, bonding pads, and corresponding connection traces. Ti was used here to improve the adhesion between parylene C and Au. Next, an array of  $8\ \mu\text{m} \times 20\ \mu\text{m}$  parylene openings was etched via  $\text{O}_2$  plasma. In the next step, through the parylene C windows, the silicon substrate was selectively etched by isotropic gas-phase etchant  $\text{XeF}_2$  as illustrated in Fig. 2(c). The depth of the undercut was measured to be  $50\ \mu\text{m}$  in this case. Larger depth can be achieved by increasing the exposure time to  $\text{XeF}_2$  or using DRIE (Deep Reactive Ion Etching) to deepen the openings before  $\text{XeF}_2$  etching. These cavities define the shape of parylene balloons. Another layer of parylene C film was conformally deposited on the bottom and side walls of the cavities as shown in Fig. 1(d). This parylene C layer simultaneously sealed the perforated top parylene C film and encapsulated the metal heaters. Oxygen plasma was then used to pattern the parylene layer to define individual devices and expose the contact pads as shown in Fig. 1(e). Finally, the backside of the wafer was patterned and etched via DRIE to form the silicon islands and release the flexible parylene balloon creases as demonstrated in Fig. 1(f). Note that the balloons extend into the silicon islands. This actually provides cushions between the metal traces and the rigid edge of silicon islands, significantly reducing stress concentration as demonstrated in our previous work.<sup>16</sup> As can be observed, the process is post-MEMS and post-CMOS compatible. All the post-processes are low-temperature ones which have excellent compatibility with MEMS sensors and CMOS circuits already fabricated on the silicon wafer. In this proof-of-concept work, no real devices are integrated on the silicon substrate. Previously, the integration of CMOS and shear-stress sensors has been demonstrated.<sup>13,14</sup>

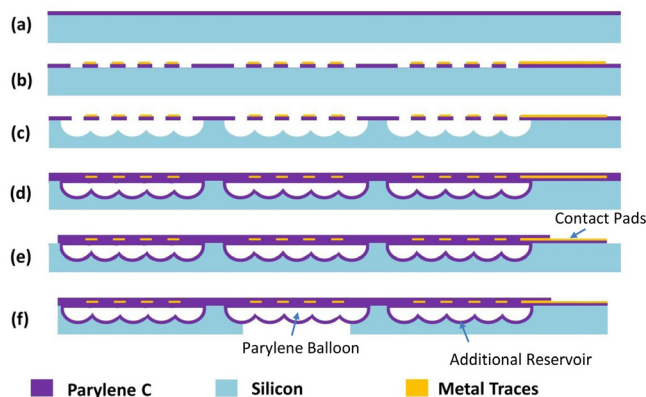
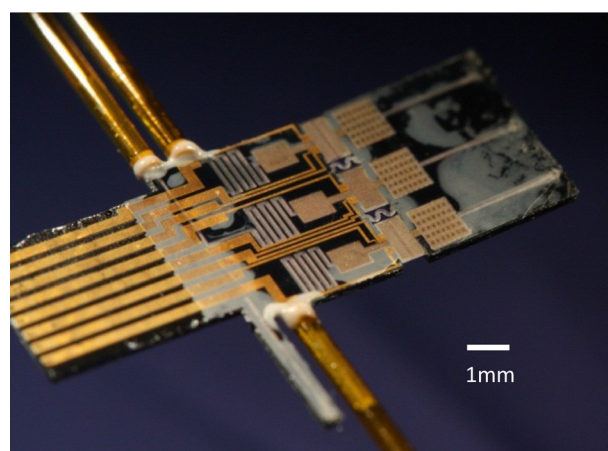


FIG. 2. Simplified fabrication process.

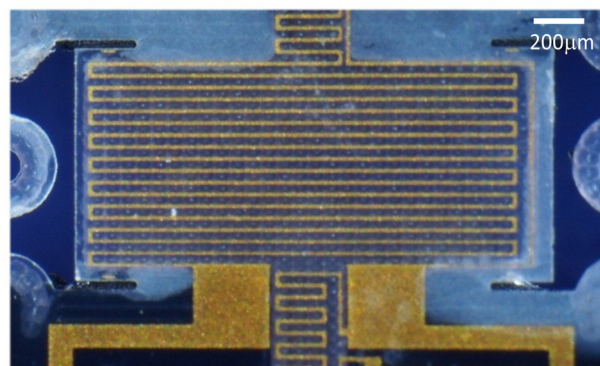
Figure 3(a) is a micrograph of a fabricated device. Since the present work is to demonstrate the self-locking and self-deploying features, the testing device only contains two silicon islands that are connected by 3 parallel parylene balloons. The integrated heaters can be accessed by the bonding pads placed on the left side. Polyimide tubes were glued for the injection of melted wax. The detail of the integrated heater can be observed in Fig. 3(b). More details of the parylene balloon can be found in the front side and back side SEM images shown in Fig. 4. Note that the parylene balloon was cut in the middle using a razor blade in order to observe the cross section.

The balloons need to be filled with paraffin wax for the self-locking and self-deploying functions. This was achieved by placing the whole device on a hotplate with the temperature set at  $60^\circ\text{C}$ , above the melting point of the paraffin wax (327212, Sigma-Aldrich). The melted wax was then simply injected via a syringe. The filling was stopped once excessive wax was observed on the outlet of the channel.

The stiffness of the parylene balloon with melted and solidified wax was measured. The test was carried out by using a needle to push against one silicon island, while the other island was clamped. The distance between needle tip and the center of the balloon was about  $4.3\ \text{mm}$ . A load cell (GS0-10 from Transducer Techniques) was used here to measure the force. The displacement was controlled by a linear actuator with a resolution of  $5\ \mu\text{m}$  in step size. In order to

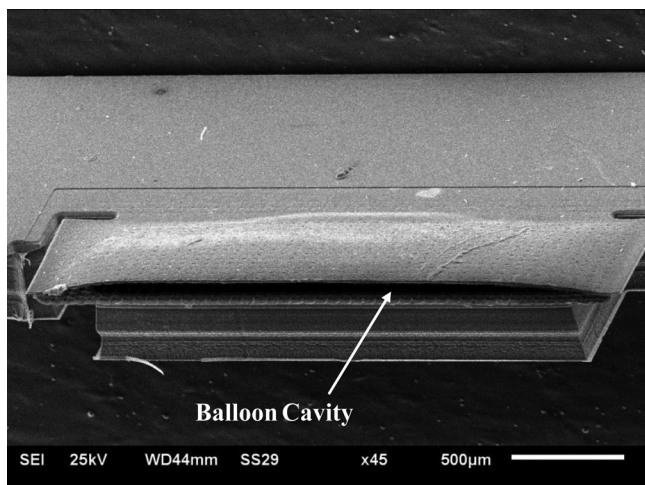


(a)

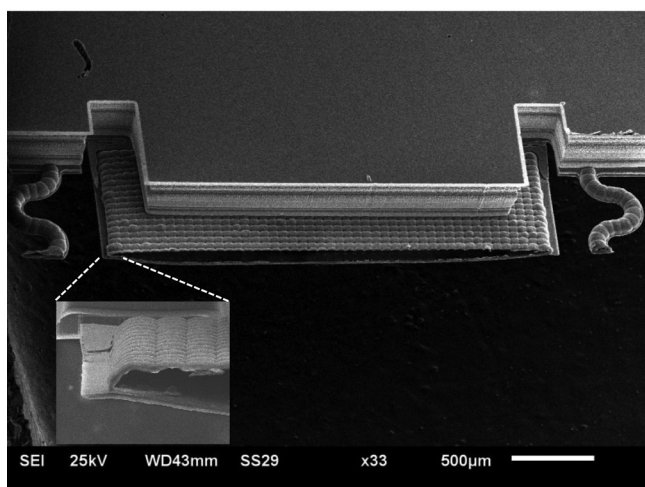


(b)

FIG. 3. (a) Front side micrograph of a fabricated micro origami structure with three wax-filled parylene balloons; (b) micrograph of the metal heater integrated on the parylene balloon.



(a)



(b)

FIG. 4. (a) Front side and (b) backside SEM images of a parylene balloon cut to show its cross section. The inset shows the enlarged view of the balloon edge.

characterize the property of a single parylene balloon, the other two balloons placed outside were removed during the experiment. Two measurements were carried out when the heater was turned on and off, respectively. The results are plotted in Fig. 5. It can be observed that the stiffness of the parylene balloon with solid wax is more than four times of the one with melted wax. In order to verify our experimental result, COMSOL Multiphysics 4.3b was used for a finite element simulation. Note that the Young's modulus of the paraffin wax can range from 1 to 4 GPa depending on its composition. In the simulation, in order to have 4 times increase in stiffness, a value of 1.8 GPa was used, which falls within the expected range of Young's modulus of paraffin wax. To have a large stiffness increase, a thicker parylene balloon can be used.

In order to estimate the temperature when the heater is on, the temperature coefficient of resistance (TCR) of the gold heater was characterized and found to be 0.00321(1/°C). When the heater was turned on by applying a constant voltage, the resistance of the heater was simultaneously monitored. Then, the temperature of the heater can be derived based on TCR.

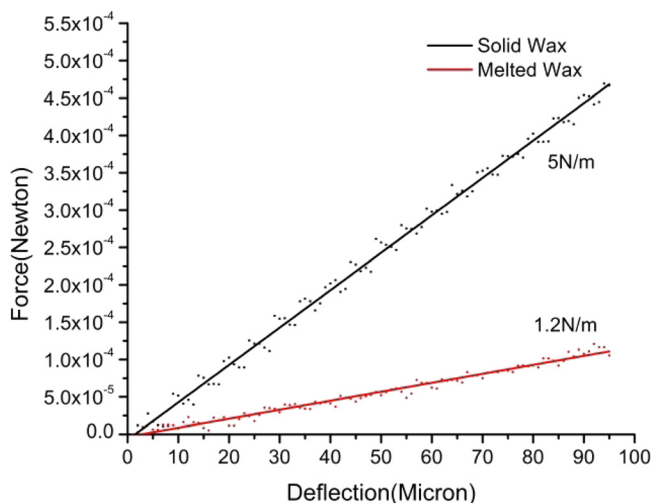


FIG. 5. Stiffness measurements of the parylene balloon with solid and melted wax.

The self-locking and self-deploying tests were carried out under a stereo microscope and recorded by a video camera. First, the heater was turned on and a micromanipulator was used to push the device into the folded state. Then, the heater was turned off while the device was kept in the folded state by the micromanipulator. After about 30 s, which is longer than the thermal time constant of the system (about 10 s), the micromanipulator was removed. Since the wax was solidified, the folding state was locked as shown in the 0 s snap shot of Fig. 6. Then, the heater was turned on, melting the paraffin wax filled inside the parylene balloon. The device returned to its original position due to the restoring force of the parylene balloon. Figure 6 shows a series of snap shots of the device when the heater was turned on at 0 s.

For the present device, the metal heater failed when the bending angle is greater than 45°. This angle can be easily increased by using longer balloons or serpentine shape balloons. The Si island and parylene balloon structure have another advantage of self-folding by utilizing the volume expansion of wax inside the balloon. In fact, in Fig. 1, there are additional wax reservoirs on the silicon islands. The reservoir (with heater) on the right island is used to provide additional volume expansion during actuating. The small reservoir (with heater) on the left island is actually a venting valve to control the pressure of the crease balloon. This Letter, however, focuses on the self-locking and self-deploying, and the self-folding feature will be implemented in our future work.

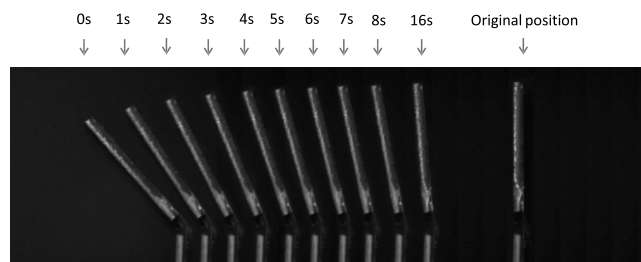


FIG. 6. Snap shots of the device during a self-deploying process after the heater was turned on at 0 s.

In conclusion, an origami platform with self-locking and self-deploying features has been demonstrated. These features are made possible by wax filled parylene balloon creases with metal heaters integrated to control the solid/liquid phases of the wax. It is possible to fill the parylene balloon with other functional polymers, further improving the functionality of this platform. The microfabrication process is post-CMOS and post-MEMS compatible, enabling the monolithic integration of electronics and sensors on the origami substrate (i.e., silicon islands). Even though there are no functional devices fabricated in this proof-of-concept work, the integration of CMOS electronics and shear-stress sensors on silicon islands has been demonstrated previously.<sup>13,14</sup> Such an origami platform, with its capabilities to self-lock, self-deploy, and monolithically integrate CMOS circuits and MEMS sensors, will be desirable for the development of many origami devices. One good example is foldable wings for micro aerial vehicles (MAVs). Note that it is highly desirable to make wings foldable to minimize the package size of MAVs. In addition, it is required that the wings can be self-deployed and locked for convenient operation. The compatibility with MEMS technology allows easy integration of flow sensors on the origami wings to study or better control the aerodynamics of micro flapping wings.

This material is based upon work partially supported by the National Science Foundation under Grant No. 1028564. H.J. and H.Y. acknowledge the seed funding from the Fulton Schools of Engineering at ASU. Any opinions, findings, and conclusions or recommendations expressed in this material

are those of the author(s) and do not necessarily reflect the views of the National Science Foundation. The microfabrication was carried out in the nFAB cleanroom at Wayne State University.

- <sup>1</sup>J. P. Gardner, J. C. Mather, M. Clampin, R. Doyon, M. A. Greenhouse, H. B. Hammel, J. B. Hutchings, P. Jakobsen, S. J. Lilly, and K. S. Long *et al.*, *Space Sci. Rev.* **123**, 485–606 (2006).
- <sup>2</sup>K. Kuribayashi, K. Tsuchiya, Z. You, D. Tomus, M. Umamoto, T. Ito, and M. Sasaki, *Mater. Sci. Eng., A* **419**, 131–137 (2006).
- <sup>3</sup>E. Hawkes, B. An, N. M. Benbernou, H. Tanaka, S. Kim, E. D. Demaine, D. Rus, and R. J. Wood, *Proc. Natl. Acad. Sci. U.S.A.* **107**, 12441–12445 (2010).
- <sup>4</sup>Y. Zhao, M. S. Nandra, and Y. C. Tai, in *Proceedings of the 16th International Conference on Solid-State Sensors, Actuators, and Microsystems (TRANSDUCERS)* (2011), pp. 2172–2175.
- <sup>5</sup>A. Vorob'ev, P. Vaccaro, K. Kubota, S. Saravanan, and T. Aida, *Jpn. J. Appl. Phys., Part 1* **42**, 4024–4026 (2003).
- <sup>6</sup>A. Azam, K. E. Laffin, M. Jamal, R. Fernandes, and D. H. Gracias, *Biomed. Microdevices* **13**, 51–58 (2011).
- <sup>7</sup>J. K. Paik, E. Hawkes, and R. J. Wood, *Smart Mater. Struct.* **19**, 125014 (2010).
- <sup>8</sup>Q. Ge, H. J. Qi, and M. L. Dunn, *Appl. Phys. Lett.* **103**, 131901 (2013).
- <sup>9</sup>L. Ionov, *Soft Matter* **7**, 6786–6791 (2011).
- <sup>10</sup>C. M. Yakacki, *Polym. Rev.* **53**, 1–5 (2013).
- <sup>11</sup>S. M. Felton, M. T. Tolley, B. Shin, C. D. Onal, E. D. Demaine, D. Rus, and R. J. Wood, *Soft Matter* **9**, 7688–7694 (2013).
- <sup>12</sup>Y. Liu, J. K. Boyles, J. Genzer, and M. D. Dickey, *Soft Matter* **8**, 1764–1769 (2012).
- <sup>13</sup>Y. Xu, F. Jiang, S. Newbern, A. Huang, C. M. Ho, and Y. C. Tai, *Sens. Actuators, A* **105**, 321–329 (2003).
- <sup>14</sup>Y. Xu, Y. C. Tai, A. Huang, and C. M. Ho, *J. Microelectromech. Syst.* **12**, 740–747 (2003).
- <sup>15</sup>H. Tu and Y. Xu, *Appl. Phys. Lett.* **101**, 052106 (2012).
- <sup>16</sup>E. Kim, H. Tu, C. Lv, H. Jiang, H. Yu, and Y. Xu, *Appl. Phys. Lett.* **102**, 033506 (2013).